

1 **High injection rates counteract formation of far-reaching fluid migration pathways**
2 **at The Geysers geothermal field**

3
4 **Stanisław Lasocki¹, and Beata Orlecka-Sikora¹**

5 ¹Institute of Geophysics Polish Academy of Sciences.

6 Corresponding author: Stanisław Lasocki (lasocki@igf.edu.pl)

7 **Key Points:**

- 8 • Degree of seismic sources disorder correlates with injection rate and amplitudes of its
9 changes agree with injection rate changes.
- 10 • Formation of long pathways for fluid migration requires certain ordering of seismic
11 sources.
- 12 • High injection rates increase sources disorder hence decrease chance for seismic fractures
13 to coalesce into long fluid migration pathways.
14

15 **Abstract**

16 Deep underground water injections induce seismicity. When the seismic fractures coalesce into
17 far-reaching pathways for fluid migration, the migrating fluid may reach pre-existing faults, and
18 by decreasing fault strength, can trigger major seismic events. We assume that the potential for
19 building such pathways depends on closeness of hypocenters, similarity of fracture planes
20 orientations, and closeness of radii taking off from the injection point, on which events locate.
21 We define this potential as the average distance between seismic events in the space of
22 parameters quantifying the above conditions. We show that in the studied case from The Geysers
23 geothermal field, this potential is highly correlated with injection rate. When the overall level of
24 injection rate is high, the higher the injection rate, the more the potential for building far-
25 reaching pathways for fluid migration is reduced.

26 **Plain Language Summary**

27 Geothermal energy production is often based on pumping cold water down to hot rocks and
28 taking back steam. Pressurized underground water injections induce brittle fracturing of rocks,
29 that is seismic events, what enhances the rock permeability and in this way increases the surface
30 on which heat exchange takes place. However, the seismic fractures may also coalesce into
31 undesired pathways enabling the fluids to migrate far and reach pre-existing tectonically
32 preloaded faults. Then the fluids decrease fault strength, and in result the fault can rupture
33 producing a major seismic event. We studied how some properties of the seismicity induced by
34 injections of water in a part of the Geysers, which can lead to the mentioned undesired fracture
35 network development, depend on injection rates. Our studies indicated that the potential for such
36 network development is highly correlated with the injection rate. Moreover, it turned out that in
37 order to avoid this unwanted development of fracture network the injection rates should be kept
38 high. The higher the injection rate is, the more the potential for building far-reaching pathways
39 for fluid migration is reduced. These results, when confirmed on other seismically active
40 geothermal energy production cases can have important implications for strategies of
41 geothermics.

42 **1 Introduction**

43 Deep underground water injections induce seismicity. This seismic fracturing of rocks is
44 desirable as it increases the surface on which heat exchange takes place in Enhanced Geothermal
45 Systems, and enhances the rocks permeability in hydrocarbon extractions based on
46 hydrofracturing. However, the seismic fractures may also coalesce into undesired pathways for
47 fluid migration. These are such pathways that enable the fluids to reach pre-existing faults. In
48 result, by decreasing fault strength, the fluids can trigger ruptures and produce major seismic
49 events. The further the migration pathways extend from the injection point, the more probable
50 are these unwanted effects. It is therefore of paramount importance to recognize under which
51 injection conditions an induced seismic process can produce such pathways (e.g.: Davies et al.,
52 2013; Ellsworth, 2013; Majer et al., 2012; Zhang Dongxiao & Yang Tingyun, 2015).

53 Numerous studies indicate that the geometry of fractures and the structure of fracture
54 networks are the main factors controlling fluid flow and the fluid transport characteristics of
55 rocks (e.g.: Hope et al., 2015; Lee et al., 1990; Long & Billaus, 1987; Schwartz et al., 1983;
56 Snow, 1965). The development of the fracturing process has been investigated in a number of
57 laboratory experiments (e.g.: Ko & Kemeny, 2011; Lockner et al., 1992; Stanchits et al., 2006).

58 Based on these experiments, many models have been developed to simulate the geometry of
59 fractures and the topology of fracture networks (e.g.: Hope et al., 2015; Lee et al., 1990; Long &
60 Billaus, 1987). However, although seismic field data provide direct insight into the development
61 of fracture networks at the crustal scale, there are few studies focused on this topic (e.g.:
62 Chorozoglou et al., 2018; Orlecka-Sikora et al., 2019; Sausse et al., 2010).

63 Here we study seismic and injection data from a part of the Geysers geothermal field to
64 determine a relation between the injection conditions and the potential of injection-induced
65 seismicity to build far-reaching pathways for fluid migration. We formulate three conditions
66 determining this potential: 1. Closeness of hypocenters; the closer the sources are to each other,
67 the higher the likelihood that they will connect. 2. Similarity of fracture plane orientation; the
68 system of linked fractures is more extended in length when the rupture planes of the fractures are
69 oriented more parallel. 3. Closeness of radii, which begin at the open hole section of the injection
70 well and on which events occur; the system of linked fractures reaches farther from the open hole
71 when the seismic sources are located on radii close to each other.

72 Consequently, seismic events are represented by eight parameters: three hypocentral
73 coordinates, three independent angles determining orientations of the T and P axes of the double-
74 couple (DC) focal mechanisms, and two angular coordinates of hypocenters in the spherical
75 system beginning at the open hole of injection well. To achieve the same scaling of these
76 parameters, we transform them to equivalent dimensions (Lasocki, 2014; Supporting Information
77 Text S1). The potential for building the far-reaching fluid migration pathways is quantified by
78 the average distance between the events in the 8-dimensional space of the aforementioned
79 parameters. When this average distance, which we refer to as the degree of disordering of
80 sources, ZZ , decreases, the potential for building the pathways increases.

81 We show that the degree of disordering of sources, ZZ , is highly significantly correlated
82 with the injection rate. ZZ took the highest values when the injection rates were the highest,
83 which indicates counterintuitively that high injection rates counteracted the formation of far-
84 reaching fluid migration pathways.

85 **2 Data and Methods**

86 The Geysers geothermal field is located in northern California, US. Geothermal
87 operations, which began there in the 1960s, and which presently use EGS technology, have
88 induced hundreds of thousands of seismic events. We studied injection and seismic data from an
89 isolated part of the field of $2\text{ km} \times 2\text{ km}$ dimension in the NW part of The Geysers, between 10
90 December 2007 and 23 August 2014. The basis for the seismic dataset was an improved catalog
91 that contained 1252 events (Kwiatek et al., 2015; Martínez-Garzón et al., 2014; 2016). This
92 unique catalog provided all the event parameters, necessary for the calculation of the degree of
93 disordering of sources, ZZ : hypocenter locations with an accuracy of 50 m, and focal
94 mechanisms with an accuracy of $20^\circ/5^\circ/10^\circ$ for strike/dip/rake. The focal mechanisms were
95 recalculated using HASH software assuming a double-couple shear source (Hardebeck &
96 Shearer, 2002; Kwiatek et al., 2015; Martínez-Garzón et al., 2016) and were used to recover the
97 trend and plunge angles of the T and P axes. The moment magnitude was used and the
98 completeness level was $M_c=1.4$ (Kwiatek et al., 2015).

99 In the study period, the injections in the study area were carried out into two wells: Prati9
100 and Prati29. There were three phases of the injection activity:

- 101 • Phase F1 from 10 December 2007 to 10 April 2010, in which only Prati9 was
 102 operational,
 103 • Phase F2 from 11 April 2010 to 21 June 2013 with simultaneous injections into both
 104 wells,
 105 • Phase F3 from 11 June 2013 to the end of the study period (23 August 2014), in which
 106 again only Prati9 was operational.

107 The injection data consisted of the daily injection volumes into Prati9 and Prati29.

108 The 1252 events formed two distinct spatial clusters: cluster A located around the open
 109 hole of Prati9 well and cluster B comprising events located closer to the open hole of Prati29
 110 well (see: Supporting Information Figure S1). We studied more numerous cluster A, consisting
 111 of 1121 events. We expected that this cluster, being spatially related to the open hole of Prati9
 112 well, was also physically related primarily to the injection activity in Prati9.

113 The parameter used here to quantify the potential for building the far-reaching fluid
 114 migration pathways, called as the degree of disordering of sources, ZZ , was the average distance
 115 between the seismic events in the 8-dimensional parameter space $\{x_1, x_2, x_3, plu_X_1, plu_X_2,$
 116 $tre_X_1, \Theta, \varphi\}$. $x_{1,2,3}$ were hypocenter coordinates. plu_X_1 and tre_X_1 were plunge and trend
 117 angles of the T axis. plu_X_2 was a plunge angle of the P axis. Θ, φ were the polar and azimuthal
 118 angles of hypocenter in the spherical system of coordinates beginning at the open hole of Prati9
 119 well. $\Theta=0$ for the vertical direction and $\varphi=0$ for the N direction. These parameters were not
 120 comparable. For this reason, we first transformed them to equivalent dimensions (ED). The
 121 transformation to ED is a technique based on a probabilistic equivalence of the parameters that
 122 scale differently (Lasocki, 2014 and Supporting Information Text S1). All transformed
 123 parameters are uniformly distributed in [0,1] and the distance between any two objects is the
 124 Euclidean metric. Further on the symbols $x_1, x_2, x_3, tre_X_1, tre_X_2, plu_X_1, plu_X_2, \Theta, \varphi$ denote
 125 the equivalent dimensions of the original source parameters.

126 The closeness of hypocenters was unequivocally parameterized by the absolute
 127 differences between hypocenter coordinates, $\Delta x_k(i, j) = |x_k(i) - x_k(j)|, k = 1, 2, 3$.

128 The trend angle and the polar angle take values in $[0^\circ, 180^\circ]$, which is $[0, 1]$ in ED, and
 129 the azimuthal angle takes values in $[0^\circ, 360^\circ]$, which is also $[0, 1]$ in ED. The shortest distances
 130 between these angles in ED were therefore:

$$131 \Delta tre_X_1(i, j) = 2 \begin{cases} |tre_X_1(i) - tre_X_1(j)| & \text{if } |tre_X_1(i) - tre_X_1(j)| \leq 0.5 \\ 1 - |tre_X_1(i) - tre_X_1(j)| & \text{if } |tre_X_1(i) - tre_X_1(j)| > 0.5 \end{cases} \quad (1)$$

$$132 \Delta \theta(i, j) = 2 \begin{cases} |\theta_i - \theta_j| & \text{if } |\theta_i - \theta_j| \leq 0.5 \\ 1 - |\theta_i - \theta_j| & \text{if } |\theta_i - \theta_j| > 0.5 \end{cases}, \quad (2)$$

$$133 \Delta \varphi(i, j) = 4 \begin{cases} |\varphi(i) - \varphi(j)| & \text{if } |\varphi(i) - \varphi(j)| \leq 0.25 \\ 0.5 - |\varphi(i) - \varphi(j)| & \text{if } 0.25 < |\varphi(i) - \varphi(j)| \leq 0.75 \\ 1 - |\varphi(i) - \varphi(j)| & \text{if } |\varphi(i) - \varphi(j)| > 0.75 \end{cases}. \quad (3)$$

134 The multipliers in front of the opening braces in equations (1-3) were inserted so that the
 135 differences in all parameters scaled in $[0, 1]$.

136 The plunge angle takes values in $[0^\circ, 90^\circ]$; hence, $\Delta plu_X_k(i, j)$ was always $|plu_X_k(i) -$
 137 $plu_X_k(j)|, k=1, 2$.

138 For a collection of n seismic sources the degree of disordering of sources, ZZ reads:

$$139 \quad ZZ = \left\{ \sum_{i=1}^{n-1} \sum_{j=i+1}^n ZZ(i, j) \right\} / \frac{n(n-1)}{2} \quad (4)$$

140 where

$$141 \quad ZZ(i, j) =$$

$$142 \quad \sqrt{\frac{[\sum_{k=1}^3 \Delta x_k(i, j)^2] + [\Delta tre_X_1(i, j)^2 + \sum_{k=1}^2 \Delta plu_X_k(i, j)^2] + [\Delta \theta(i, j)^2 + \Delta \varphi(i, j)^2]}{\Delta_r(i, j)^2 + \Delta_M(i, j)^2 + \Delta_\phi(i, j)^2}} =$$

$$143 \quad \sqrt{\Delta_r(i, j)^2 + \Delta_M(i, j)^2 + \Delta_\phi(i, j)^2} \quad (4a)$$

144 $\Delta_r(i, j)$ is the distance between hypocenters of events i and j ;

145 $\Delta_M(i, j)$ is the distance between focal mechanisms of these two events;

146 $\Delta_\phi(i, j)$ is the distance between the directions of radii from the Prati9 open hole, those on
147 which the hypocenters of these two events locate.

148 We carried out our analyses separately in the three injections phases. Out of 1121 studied
149 events, 248 events occurred in the injection phase F1, 702 events – in the phase F2 and 171
150 events – in the phase F3. For every injection phase we calculated ZZ for 50-event window sliding
151 by 10 events. The number of events per phase was not high enough to use non-overlapping
152 windows. For sliding windows we obtained 21 ZZ values for F1, 66 ZZ values for F2 and 13 ZZ
153 values for F3.

154 Next, we calculated the average injection rates, IN , during time windows covering the
155 periods of the 50-event sliding windows, respectively. The calculations were performed for the
156 injection rate periods exactly matching the periods of respective 50-event windows and for the
157 injection rate periods from 1 to 21 days preceding the periods of event windows. The latter part
158 of this analysis was meant to study delayed reactions of seismicity.

159 Finally, we studied the correlation between ZZ – values and IN – values. It comes from
160 equation (4a) that ZZ is composed of three components representing our three conditions
161 determining the potential of injection-induced seismicity for building far-reaching pathways for
162 fluid migration. In order to recognize contributions of these components to the correlations
163 between ZZ and IN we studied also the correlations between $\Delta_r, \Delta_M, \Delta_\phi$ – values and IN – values,
164 respectively.

165 All correlation analyses were preceded by the Jarque-Bera test applied to check normality
166 of the distributions of the used variables. If the normality hypothesis was not rejected we used
167 the Person's correlation; in rare otherwise cases we used the Spearman rank correlation.

168 We also tested differences between the values of location parameters by phase of IN, ZZ ,
169 seismic activity rate and magnitude, respectively. When the normality hypothesis for a parameter
170 was not rejected, we used the Student's t-test for means, otherwise we applied the Mann-
171 Whitney U-test for medians. All statistical inferences were performed under the significance
172 level $\alpha=0.05$.

173 **3 Results and Discussion**

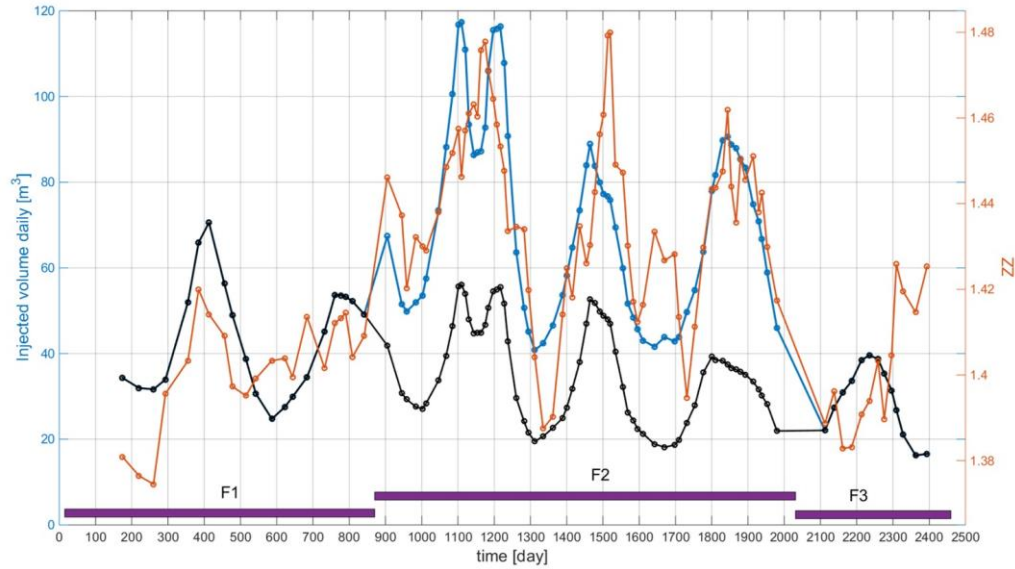
174 Some descriptive statistics by phase of *IN*, *ZZ*, seismic activity rate and magnitude of
 175 events are presented in Table 1 together with comparisons of their location parameters (means or
 176 medians) among phases. The medians of injection rates into Prati9 well were decreasing
 177 statistically significantly with injection phase.

178 **Table 1.** Descriptive statistics and comparisons of the average injection rate, *IN*, the degree of
 179 disordering of seismic sources, *ZZ*, the activity rate, and magnitude of events in the three
 180 injection phases. The magnitude was transformed to the equivalent dimension. The statistics of
 181 these parameters concern their respective values from sliding event windows. The column
 182 “Comparisons” contains *p*-values of the tests of differences between means or medians of these
 183 parameters. The significant differences are in bold.

| | Injection phase | | | | | | | | | Comparisons of location parameters, <i>p</i> -value | | |
|--|-----------------|-------|-----------|-------|-------|-----------|-------|-------|-----------|---|--------------|-------------|
| | F1 | | | F2 | | | F3 | | | F1 vs. F2 | F2 vs. F3 | F1 vs. F3 |
| | Mean | Med. | Std. dev. | Mean | Med. | Std. dev. | Mean | Med. | Std. dev. | | | |
| Prati9 <i>IN</i> [100m ³ /day] | 43.76 | 45.18 | 13.09 | 36.18 | 35.69 | 11.51 | 29.10 | 30.95 | 8.18 | 0.024 | 0.014 | 3E-4 |
| Summed Prati9 and Prati29 <i>IN</i> [100m ³ /day] | 43.76 | 45.18 | 13.09 | 72.82 | 73.43 | 22.54 | 29.10 | 30.95 | 8.18 | ----- | | |
| <i>ZZ</i> | 1.402 | 1.403 | 0.012 | 1.439 | 1.438 | 0.021 | 1.401 | 1.396 | 0.015 | 5E-14 | 2E-7 | 0.91 |
| Activity rate [event/day] | 0.35 | 0.34 | 0.13 | 0.70 | 0.69 | 0.23 | 0.48 | 0.44 | 0.11 | 7E-12 | 6E-6 | 7E-3 |
| Magnitude | 0.55 | 0.57 | 0.06 | 0.49 | 0.49 | 0.04 | 0.45 | 0.47 | 0.06 | 3E-4 | 0.055 | 2E-4 |

184
 185

186 Figure 1 compares the time-variations in the degree of disordering of sources, *ZZ*, with
 187 the variations of the average injection rate, *IN*. In phase F2 this comparison concerns the
 188 injection rate into Prati9 well, *IN*(9), and the total injection rate into both wells, *IN*(both). It is
 189 seen in the figure that in the first two injection phases, F1, F2, *ZZ* correlated positively with *IN*.
 190 Also the amplitudes of the *ZZ*-changes agreed well with the amplitudes of the average injection
 191 rate changes. In phase F2, this agreement related to the summed injection into both wells (blue
 192 curve) rather than Prati9 well alone (black curve), even though the analyzed seismic events were
 193 geometrically linked to Prati9 (Supporting Information Figure S1).



194

195 **Figure 1.** Comparison of the time-variation of the degree of disordering of sources, ZZ , with the
 196 time-changes of average injection rate. Black – the injection rate into Prati9 well, blue – the total
 197 injection rate into Prati9 and Prati29 wells, brown – ZZ . The horizontal bars mark the durations of
 198 the three injection phases. The injection rate values are the daily injection volumes averaged over
 199 the times covered by the event windows, respectively.

200

201 Table 2 presents the results of analysis of correlations between the injection rate, IN , and
 202 the degree of disordering of sources, ZZ . These results confirm the correlations evidenced in
 203 Figure 1. In F1 and F2 the correlation between IN and ZZ was significant, positive. In F2 this
 204 correlation was highly significant, irrespective of whether the IN referred to injections into Prati9
 205 or to the summed injections into Prati9 and Prati29 wells.

206 **Table 2.** Results of the correlation analysis between the average injection rate, IN , and the degree
 207 of disordering of seismic sources, ZZ , and its components, Δ_r , Δ_M , Δ_ϕ . For the phase F2 row ‘a’
 208 provides the correlation between ZZ and IN into Prati9 well, and row ‘b’ provides the correlation
 209 between ZZ and total IN into Prati9 and Prati29 wells. The significant correlations are in bold.
 210 The results based on Spearman rank correlation are in italics.

| Injection phase | ZZ | | Δ_r | | Δ_M | | Δ_ϕ | |
|-----------------|--------------|--------------------------------------|-------------|--------------------------------------|-------------|-------------------------------------|---------------|-------------------------------------|
| | Corr. coef. | p -value | Corr. coef. | p -value | Corr. coef. | p -value | Corr. coef. | p -value |
| F1 | 0.62 | 0.002 | 0.69 | $5 \cdot 10^{-4}$ | 0.20 | 0.37 | -0.28 | 0.22 |
| F2 – a | 0.76 | $2 \cdot 10^{-13}$ | 0.69 | $2 \cdot 10^{-10}$ | 0.41 | $7 \cdot 10^{-4}$ | 0.49 | $3 \cdot 10^{-5}$ |
| F2 – b | 0.72 | $7 \cdot 10^{-12}$ | 0.65 | $1 \cdot 10^{-9}$ | 0.45 | $1 \cdot 10^{-4}$ | 0.47 | $8 \cdot 10^{-5}$ |
| F3 | -0.60 | 0.029 | -0.20 | 0.51 | -0.32 | 0.28 | -0.19 | 0.52 |

211

212 The results of correlation analysis for delayed ZZ with respect to IN are presented in
 213 Supporting Information Tables S1-S4. In F1 the correlation coefficient slowly decreases with
 214 increasing lag. The correlation coefficient in F2 slightly increased when ZZ was delayed with

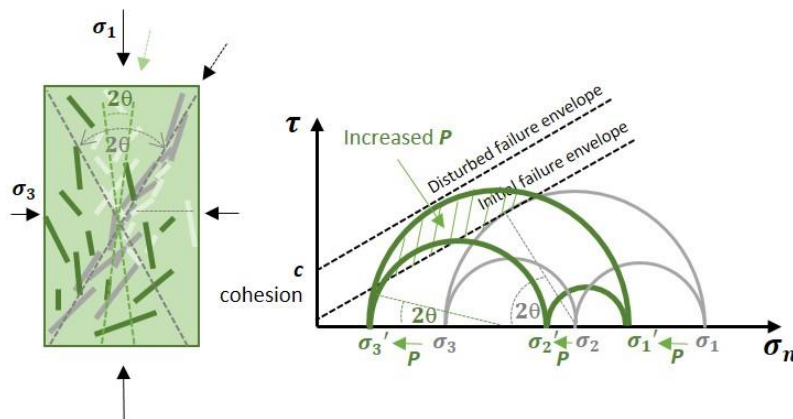
215 respect to IN , however the difference between the correlation coefficient for zero lag and for 13
 216 days lag was only 0.022 and was surely insignificant.

217 The previous studies of the same data have indicated a positive correlation between
 218 seismicity rates and injection rates (Leptokaropoulos et al., 2018). Hence different time periods
 219 corresponded here to the 50-events windows; the time periods at higher injection rates were
 220 shorter. We checked whether the positive ZZ vs. IN correlations were not due to these differences
 221 between time periods. For this purpose we divided the F2 phase into non-overlapping windows
 222 of constant, 68 days duration. The correlation between IN and ZZ both calculated for these
 223 windows of constant time period, was also positive (0.87) and significant ($p = 0.0097$).

224 In F1 only Δ_r out of three components of ZZ (see: Data and Methods, Equation 4a)
 225 significantly and positively correlated with IN . The correlation was the highest for zero lag
 226 (Supporting Information Table S1). Hence, in this injection phase the positive $ZZ - IN$ correlation
 227 resulted from that that higher injection rates were increasing distances between the sources.
 228 However, this effect was not caused by moving away of sources from the well opening of Prati9.
 229 In neither phase the correlation coefficient between IN and the average distance of hypocenters
 230 from the open hole was significant.

231 In F2 all three distances, $\Delta_r, \Delta_M, \Delta_\phi$, were highly positively correlated with IN thus they
 232 all significantly contributed to the correlation $ZZ - IN$. Higher injection rates led to an increase of
 233 the distances between hypocenters, to a greater variety of P and T axes directions and to a greater
 234 angular dispersion of the hypocenters in relation to the open hole of Prati9 well. Nothing more
 235 interesting was obtained from the correlations when ZZ was delayed with respect to IN
 236 (Supporting Information Tables S2-S3).

237 A way in which increased injection rates may increase the degree of disordering of
 238 sources (ZZ) is shown schematically in Figure 2. An increase of pore pressure resulting from the
 239 increased injection rate broadens the range of possible orientations and locations for new shear
 240 fractures.



241
 242 **Figure 1.** Schematic presentation of influence of pore pressure (P) changes on the failure plane
 243 orientations. The linear failure criterion imposes that shear fractures make with σ_1 a well-defined
 244 angle of $(\pm) 45^\circ - \phi/2$, where ϕ is the angle of internal friction, and $\theta = \phi/2 + 45$ (gray circle in
 245 Coulomb-Mohr diagram and gray fractures on the rock block on the left). An increase of P
 246 reduces the effective normal stress, σ'_n , where $\sigma'_n = \sigma_n - P$ and broadens the range of possible

247 orientations for new shear fractures (all directions going through green hatched area in the
248 Coulomb-Mohr diagram and green fractures on the rock block) (after Warren-Smith et al., 2019).

249 The previous studies of the fracture network development, carried out on the same data,
250 have shown that the connectivity of fractures induced by fluid injection is lower for higher
251 injection rates and *vice versa* (Orlecka-Sikora et al., 2019). Thus the connectivity was responding
252 to the injection rate changes in the same way as *ZZ*. This allows for inferring that *ZZ* indeed
253 represents the potential of fluid migration. In the cited work the connectivity was estimated by
254 the connectivity coefficient, C , defined by the ratio of the observed number of intersections of
255 fractures in a fracture network to the number of all possible intersections in this network. These
256 all possible intersections were evaluated as $0.5f(f - 1)$, where f was the number of fractures
257 building the fracture network (21, 22)

258 In the F3 phase, in which the overall level of the injection rate, *IN*, was the lowest among
259 injection phases, the correlation between *IN*, and the degree of disordering of sources, *ZZ*, was
260 significant, negative. This correlation was achieved only jointly by the three components of *ZZ*:
261 Δ_r , Δ_M , Δ_ϕ because neither of the them significantly correlated with *IN* (Table 2). The negative
262 correlation coefficient in F3 increased when *ZZ* was delayed with respect to *IN*, and for 4 and
263 more days lag it became statistically not significant (Supporting Information Table S4). The
264 change of sign of the *IN* – *ZZ* correlation in F3 may be explained by the role of injection rate
265 changes on the weakening/strengthening of rock. According to rock sample studies of Fjaer and
266 Ruisten (2002) in rock weakening conditions there are many equivalent orientations of the
267 failure plane, and the fracture orientation is determined by local weaknesses of the rock. In
268 conditions of rock strengthening only two orientations for the potential failure plane fulfil the
269 Coulomb failure criterion. Thence rock weakening conditions result in poorly ordered seismic
270 fractures, and in rock strengthening conditions the fractures are better ordered. Orlecka-Sikora
271 and Cielesta (2019) found two mutually reversed reactions of the stress field to injection rate
272 changes in The Geysers, with the reversal point at some $50\text{-}70 \cdot 10^2 \text{ m}^3/\text{day}$. At injection rates
273 above this interval, increasing the injection rate enhanced rock weakening, and a decrease in the
274 injection rate led to rock strengthening. Below this interval, the effect of injection rate variation
275 was the opposite.

276 The injection rates in F1 and F2 were mostly above the aforementioned reversal point. To
277 the contrary, the injection rates in F3 were well below this point. In the first two phases,
278 weakening of the rock with increasing injection rate could favor the formation of randomly
279 oriented fractures, which was expressed by the increase in the degree of disordering, *ZZ*. In F3
280 increasing the injection rate could lead to rock strengthening, which promoted the formation of
281 fractures oriented in the optimal direction. As a consequence, the fractures were better ordered,
282 which reduced *ZZ*.

283 The second well, Prati29, was operational only in F2 phase. In this phase the amplitudes
284 of *ZZ* changes agreed with the amplitudes of changes of the summarized injections into Prati9
285 and Prati29. Furthermore, the mean level of *ZZ* and the mean seismic activity were the highest in
286 this phase and significantly higher than in phases F1 and F3. In F2 only the level of total
287 injection into Prati9 and Prati29 was the highest, and the mean level of injection rate into the
288 Prati9 well was significantly smaller than in phase F1 (see: Table 1). All these indicate the
289 important role of the injections into Prati29 for the generation of seismic events within the

290 studied cluster A in spite of the considerable distance between the open hole section of Prati29
291 well and the events from cluster A.

292 The seismic events generated at higher injection rates, i.e. the ones more disordered (*ZZ*
293 was higher), did not have greater magnitudes. On the contrary, in the F1 phase the mean
294 magnitude in windows correlated negatively with *ZZ* (corr. coef. -0.61, $p = 0.003$. In the F2
295 phase no magnitude – *ZZ* correlation was observed.

296 **4 Conclusions**

297 Studying the actual field data we found exceptionally high and immediate correlation
298 between the injection rate and the seismicity parameter - the degree of disordering of sources,
299 *ZZ*. Also the amplitudes of *ZZ*-changes agreed very well with the amplitudes of the average
300 injection rate changes. *ZZ* is defined solely on parameters of seismic sources. It describes how
301 much seismic fractures are dispersed in terms of distances between their hypocenters, mutual
302 orientations of their fracture planes, and angular dispersion of their hypocenters.

303 We interpret *ZZ* as a measure of the potential of seismic fractures for building far-
304 reaching pathways for fluid migration. The logic of the three conditions on which *ZZ* is based,
305 supports this interpretation though these conditions are certainly not adequate for all possibilities
306 of fracture network development (e.g. not for a percolating fluid pathway).

307 In the studied case from The Geysers geothermal field, the optimal conditions to avoid
308 such ordering of seismic fractures that enable linking them into longer pathways, extending
309 farther from the injection point were met for high injection rates. The higher the injection rate
310 was, the more disordered the seismic fractures were generated, i.e., the chances to build longer
311 pathways for undesired fluid migration was decreased. High injection rates caused an increase in
312 seismic activity, nevertheless the median level of seismic event magnitudes remained unaffected.

313 The above conclusion, if confirmed in other cases of injection induced seismicity, would
314 open new perspectives on managing seismic hazards and optimizing technological production.
315 Martinez-Garzon, et al. (2018) conclude that the used here dataset from the NW region of The
316 Geysers well represents the broader seismic processes at The Geysers field. Thus our results may
317 be also valid for all seismic processes at The Geysers. However, for further generalizations
318 studies of other injection-induced seismicity cases are required.

319 **Acknowledgments**

320 We thank the Calpine Corporation for providing high-resolution hydraulic data from The
321 Geysers field. This work was supported under the S4CE: "Science for Clear Energy" project,
322 which has received funding from the European Union's Horizon 2020 research and innovation
323 programme, under grant agreement No 764810. The work was also partially supported by
324 statutory activities No 3841/E-41/S/2018 of the Ministry of Science and Higher Education of
325 Poland. Data are available on the IS-EPOS platform of Thematic Core Service Anthropogenic
326 Hazards, Episode: THE GEYSERS Prati 9 and Prati 29 cluster, (https://tcs.ah-epos.eu/#episode:THE_GEYSERS_Prati_9_and_Prati_29_cluster, doi:
327 10.25171/InstGeoph_PAS_ISEPOS-2017-011).
328

329 **References**

- 330 Chorozoglou, D., Kugiumtzis, D., & Papadimitriou, E. (2018) Testing the structure of earthquake
 331 networks from multivariate time series of successive main shocks in Greece, *Physica A*, 499, 28–
 332 39.
- 333 Davies, R., Foulger, G., Bindley, A., & Styles, P. (2013) Induced seismicity and hydraulic
 334 fracturing for the recovery of hydrocarbons, *Marine and Petroleum Geology*, 45, 171-185.
- 335 Ellsworth, W.L. (2013) Injection-induced earthquakes, *Science*, 341, 6142, doi:
 336 10.1126/science.1225942
- 337 Fjaer, E., & Ruistuen, H. (2002) Impact of the intermediate principal stress on the strength of
 338 heterogeneous rock, *Journal of Geophysical Research, Solid Earth*, 107, B2, 2032, doi:
 339 10.1029/2001JB000277.
- 340 Hardebeck, J.L., & Shearer, P.M. (2002) A new method for determining first-motion focal
 341 mechanisms, *Bulletin of Seismological Society of America*, 92, 2264-2276.
- 342 Hope, S.M., Davy, P., Maillot, J., Le Goc, R., & Hansen, A. (2015) Topological impact of
 343 constrained fracture growth. *Frontiers in Physics* 3-75.
- 344 Kijko A., Lasocki S., & Graham G. (2001) Nonparametric seismic hazard analysis in mines.
 345 *Pure and Applied Geophysics*, 158, 1655-1676
- 346 Ko, T.Y., & Kemeny, J. (2011) Subcritical crack growth in rocks under shear loading. *Journal of*
 347 *Geophysical Research, Solid Earth*, 116, B01407, doi:10.1029/2010JB0008461.
- 348 Kwiatek, G., Martínez-Garzón, P., Dresen, G., Bohnhoff, M., Sone, H., & Hartline, C. (2015)
 349 Effects of long-term fluid injection on induced seismicity parameters and maximum magnitude
 350 in northwestern part of The Geysers geothermal field. *Journal of Geophysical Research, Solid*
 351 *Earth*, 120, 7085–7101, doi: 10.1002/2015JB012362.
- 352 Lasocki, S. (2014) Transformation to equivalent dimensions – a new methodology to study
 353 earthquake clustering. *Geophysical Journal International*, 197 (2), 1224-1235.
- 354 Lee, J.S., Veneziano, D., & Einstein, H.H. (1990) “Hierarchical fracture trace model” In *Rock*
 355 *Mechanics Contributions and Challenges: Proceedings of the 31st US Symposium on Rock*
 356 *Mechanics*, W. Hustrulid, W., & Johnson, G.A., Eds. (A.A. Balkema 1990), pp. 261-268.
- 357 Leptokaropoulos, K., Staszek, M., Lasocki, S., Martínez-Garzón, P., & Kwiatek, G. (2018)
 358 Evolution of seismicity in relation to fluid injection in the North-Western part of The Geysers
 359 geothermal field. *Geophysical Journal International*, 212, 1157–1166, doi: 10.1093/gji/ggx481
- 360 Lockner, D.A., Byerlee, J., Kuksenko, V., Ponomarev, A., & Sidorin, A. (1992) “Observations of
 361 quasi-static fault growth and acoustic emissions” in *Fault Mechanics and Transport Properties of*
 362 *Rocks*, B. Evans and T.-F. Wong, Eds. (Academic, London 1992), pp. 3–31.
- 363 Long, J.C.S., & Billaus, D.M. (1987) From field data to fracture network modeling: An example
 364 incorporating special structure, *Water Resources Research*, 23(7), 1201-1216.
- 365 Majer, E., Nelson, J., Robertson-Tait, A., Savy, J., & Wong, I. (2012) Protocol for Addressing
 366 Induced Seismicity Associated with Enhanced Geothermal Systems, *Geothermal Technologies*
 367 *Program U.S. Department of Energy, Energy Efficiency & Renewable Energy*
- 368 Martínez-Garzón, P., Kwiatek, G., Bohnhoff, M., & Dresen, G. (2016) Impact of fluid injection
 369 on fracture reactivation at The Geysers geothermal field, *Journal of Geophysical Research. Solid*
 370 *Earth*, 121(10), 7432–7449, doi: 10.1002/2016JB013137.
- 371 Martínez-Garzón, P., Kwiatek, G., Sone, H., Bohnhoff, M., Dresen, G., & Hartline, C. (2014)
 372 Spatiotemporal changes, faulting regimes, and source parameters of induced seismicity: A case
 373 study from The Geysers geothermal field. *Journal of Geophysical Research. Solid Earth*, 119,
 374 8378–8396, doi: 10.1002/2014JB011385.

- 375 Martínez-Garzón, P., Zaliapin, I., Ben-Zion, Y., Kwiatek, G. & Bohnhoff, M. (2018)
376 Comparative study of earthquake clustering in relation to hydraulic activities at geothermal fields
377 in California. *Journal of Geophysical Research. Solid Earth*, **123**.
- 378 Orlecka-Sikora, B. & Cielesta, S. (2019) Evidence that the injection-induced earthquakes rupture
379 subcritically. *Scientific Reports* (submitted)
- 380 Orlecka-Sikora, B. & Lasocki, S. (2005) “Nonparametric characterization of mining induced
381 seismic sources.” In: Proceedings Sixth International Symposium on Rockburst and Seismicity in
382 Mines 9-11 March 2005, Australia, Potvin, Y., & Hudyma, M., Eds. (Australian Centre for
383 Geomechanics, Nedlands 2005), pp. 555-560
- 384 Orlecka-Sikora, B., Cielesta, S., & Lasocki, S. (2019) Tracking the development of seismic
385 fracture network from The Geysers geothermal field. *Acta Geophysica*, *67*, 341-350.
- 386 Sausse, J.C., Dezayes, C., Dorbath, L. Genter, A., & Place, J. (2010) 3D model of fracture zones
387 at Soultz-sous-Forêts based on geological data, image logs, induced microseismicity and vertical
388 seismic profiles. *Comptes Rendus Geo-sciences*, *342*(7-8), 531-545.
- 389 Schwartz, F.W., Smith, L. & Crowe, A.S. (1983) A stochastic analysis of macroscopic dispersion
390 in fractured media, *Water Resources Research*, *19*(5), 1253-1265.
- 391 Silverman, B.W. (1986) “Density Estimation for Statistics and Data Analysis.” (Chapman and
392 Hall, London, 1986.)
- 393 Snow, D.T. (1965) A parallel plate model fractured permeable media, PhD. Thesis, Univ. of
394 Calif., Berkeley.
- 395 Stanchits, S., Dresen, G., & Guéguen, Y. (2006) Ultrasonic velocities, acoustic emission
396 characteristics and crack damage of basalt and granite, *Pure Applied Geophysics*, *163*(5–6), 975–
397 994.
- 398 Warren-Smith, E., Fry, B., Wallace, L., Chon, E., Henrys, S., Sheehan, A., Mochizuki, K.,
399 Schwartz, S., Webb, S. & Lebedev, S. (2019) Episodic stress and fluid pressure cycling in
400 subducting oceanic crust during slow slip. *Nature Geoscience*, *12*, 475–481,
401 doi.org/10.1038/s41561-019-0367-x
- 402 Zhang Dongxiao & Yang Tingyun (2015) Environmental impacts of hydraulic fracturing in shale
403 gas development in the United States, *Petroleum Exploration and Development*, *42*(6), 876–883.
404
405